X-ray photoelectron spectroscopy analysis of boron defects in silicon crystal: A first-principles study

Jun Yamauchi,[1] Yoshihide Yoshimoto,[2] and Yuji Suwa[3]
[1]*Faculty of Science and Technology, Keio University, 3-14-1 Hiyoshi, Yokohama 223-8522, Japan*
[2]*Department of Computer Science, Graduate School of Information Science and Technology, The University of Tokyo, 7-3-1 Hongo, Bunkyo-ku, Tokyo 113-0033, Japan*
[3]*Research and Development Group, Hitachi, Ltd., 1-280, Higashi-Koigakubo, Kokubunji-shi, Tokyo 185-8601, Japan*

(Received 11 January 2016; accepted 21 April 2016; published online 6 May 2016)

We carried out a comprehensive study on the B 1*s* core-level X-ray photoelectron spectroscopy (XPS) binding energies and formation energies for boron defects in crystalline silicon by first-principles calculation with careful evaluation of the local potential boundary condition for the model system using the supercell corresponding to 1000 Si atoms. It is reconfirmed that the cubo-octahedral B_{12} cluster in silicon crystal is unstable and exists at the saddle point decaying to the icosahedral and S_4 B_{12} clusters. The electrically active clusters without any postannealing of ion-implanted Si are identified as icosahedral B_{12} clusters. The experimentally proposed threefold coordinated B is also identified as a ⟨001⟩B-Si defect. For an as-doped sample prepared by plasma doping, the calculated XPS spectra for complexes consisting of vacancies and substitutional B atoms are consistent with the experimental spectra. It is proposed that, assuming that the XPS peak at 187.1 eV is due to substitutional B (B_s), the experimental XPS peaks at 187.9 and 186.7 eV correspond to interstitial B at the H-site and ⟨001⟩B-Si defects, respectively. In the annealed samples, the complex of B_s and interstitial Si near the T-site is proposed as a candidate for the experimental XPS peak at 188.3 eV. *Published by AIP Publishing.*
[http://dx.doi.org/10.1063/1.4948572]

I. INTRODUCTION

Boron is technologically the most important element used as the *p*-type dopant in silicon. As the size of devices on integrated circuits decreases, the high-dose ion implantation of dopant atoms into silicon is indispensable for forming shallow junctions with a high impurity concentration. Various studies on the behavior of highly dosed boron atoms have been reported.[1–3]

At high concentrations, boron atoms form clusters and precipitates, which have a marked effect on impurity diffusion and electrical activity. Implanted boron is generally considered to be initially located at interstitial sites immediately after implantation and does not act as an acceptor until an annealing process is performed. However, Mizushima *et al*. experimentally showed that ion implantation with a very high dose (10^{16} – 10^{17} cm^{-2}) results in unexpectedly low resistivity even without an annealing process, and they suggested that icosahedral (ICO) B_{12} clusters may have been responsible for the low resistivity.[4,5] First-principles calculations of the electronic structure and infrared (IR) absorption spectra supported the existence of these clusters.[6,7] In contrast, Ohmori *et al*. performed a B 1*s* core-level X-ray photoelectron spectroscopy (XPS) calculation by Slater's transition state (STS) method using the DV-Xα method for cluster models and concluded that octahedral (OCT) B_6 clusters were related to the low resistivity by comparing the calculation results with the experimental XPS data of Mizushima *et al*.[8] Later, they included cubo-octahedral (CO) B_{12} clusters as possible electrically active clusters.[9] Boron naturally forms exotic atomic configurations, including clusters such as OCT B_6 and ICO and CO B_{12}.[10]

Recently B plasma-doping has been attracting interest. Tsutsui *et al*. carried out XPS measurements at the Super Photon Ring 8 GeV (SPring-8) facility and found three characteristic peaks due to B defects.[11] Furthermore, Uedono *et al*. suggested that the major defects in a sample immediately after B-implantation by plasma immersion are divacancy-B complexes as a result of investigation using a monoenergetic positron beam as well as by XPS.[12] On the experimental side, powerful synchrotron radiation facilities have been used to measure the XPS signals of defects, which are very weak owing to the very low defect concentration. On the other hand, there have been few reliable first-principles core-level XPS calculations for impurity clusters in semiconductors, because the local potential boundary condition of defect model systems has not yet been sufficiently evaluated. To obtain reliable shifts in the XPS binding energy, it is necessary to take a sufficiently large supercell for a defect not to affect the local potential at the boundary.

In this work, we report a comprehensive study on theoretically and/or experimentally considerable defects with careful evaluation of the boundary condition, that is, the convergence of the local potential with respect to the supercell size, and we identify the defects consistent with the aforementioned experimental observations. Our preliminary results using supercells of 512 Si atoms were reported in Ref. 13. In the present study, we investigate the charged states as well as the spin polarized states, and reveal more reliable results using supercells of 1000 Si atoms.

II. CALCULATION METHOD

The calculations are based on density functional theory with the GGA PBE96 approximation.[14] The atomic configurations are fully optimized for the total energy with a force criterion of less than 1×10^{-3} Hartree/Bohr. The interactions between ions and electrons are described by a norm-conserving pseudopotential for Si[15] and an ultrasoft pseudopotential for B.[16] Unless otherwise mentioned, as described later, the calculation model is a cubic supercell with a side of approximately 2.5 nm, corresponding to a crystal containing 1000 Si atoms. The sampled k-point is the single Γ point and the cutoff energy is 25 Ry. The calculation code is xTAPP,[17] which is a highly parallelized version of the plane-wave-based code TAPP (Tokyo *ab initio* program package).[18]

For the XPS calculation, we adopt the ΔSCF method with a screened core-hole pseudopotential (SCHP)[19] as well as the STS method using a pseudopotential with core electrons (PWC). The PWCs are used to treat deep orbitals such as B 1*s* and Si 2*s* as valences, which is possible using the multireference function of the ultrasoft pseudopotential.[16,20] As a test of accuracy for the PWCs and SCHPs, we calculate the relative XPS binding energies of B 1*s* in pentaborane(9) (B_5H_9) and C 1*s* in propyne (C_3H_4), which are summarized in Table I. Experimental data are from Ref. 21. The calculation methods are the frozen orbital (FO), STS, and ΔSCF methods. In the FO method, the binding energy is the negative value of the eigenvalue of the core state. In the STS method, the binding energy is the negative value of the eigenvalue of the relevant core state whose occupation is one half electron. In the ΔSCF method, the XPS binding energy is obtained as the difference between the total energy in the state where one electron in the relevant core state is removed and that in the ground state. Among these three calculation methods, the FO method gives the worst results because it does not include the relaxation effect, which is the energy reduction caused by the relaxation of the remaining electrons after the emission of a photoelectron. Although the PWCs are less accurate than the SCHPs in this test, the PWCs enable us to calculate the XPS binding energies by the STS method and to compare the energies with the results by Ohmori *et al.*,[8,9]

TABLE I. Relative XPS binding energies (eV) of B 1*s* in pentaborane(9) (B_5H_9) and C 1*s* in propyne (C_3H_4). The calculation methods are the frozen orbital (FO), Slater's transition state (STS), and ΔSCF methods. The number following a symbol for an element indicates the atomic position. Pentaborane(9) has C_{4v} symmetry, which divides B atoms into two groups: one atom (B1) and four atoms (B2). The molecular formula of propyne is C(1)H_3-C(2)-C(3)H, where the numbers in parentheses refer to C1, C2, and C3. Experimental data are from Ref. 21.

	Calculation				
Pseudopotentials	PWC			SCHP	
Method	FO	STS	ΔSCF	ΔSCF	Exp.
B1	0.00	0.00	0.00	0.00	0.0
B2	1.58	1.69	1.67	1.90	1.9
C1	0.68	1.08	1.09	1.41	1.37
C2	0.39	0.49	0.49	0.61	0.67
C3	0.00	0.00	0.00	0.00	0.00

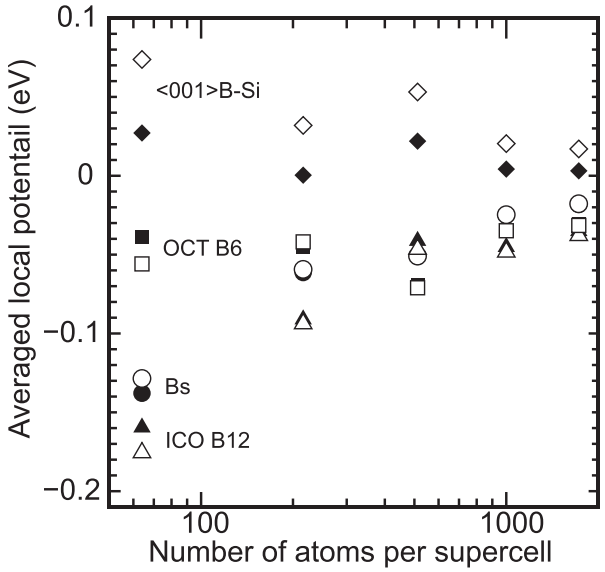

FIG. 1. Supercell size dependence of the average local potential. The potential is averaged within a sphere of radius 1.6 Bohr centered on an Si atom near the vertex of the cubic supercell. The origin is set to that of pure Si crystal for each supercell size. The horizontal axis refers to the number of atoms per supercell for pure Si crystal. The circles, triangles, squares, and diamonds indicate substitutional B (B_s), icosahedral B_{12}, octahedral B_6, and ⟨001⟩B-Si defects, respectively. Closed and open symbols refer to the neutral and charged states, respectively. The charged defects are B_s^-, ICO B_{12}^{2-}, OCT B_6^{2-}, and ⟨001⟩B-Si^+.

which are obtained using the DV-Xα and the STS methods. Unless otherwise mentioned, we adopt the ΔSCF method using the SCHP for the XPS binding energy calculation.

For the calculation of defect, we must compare the XPS binding energies for each defect in different supercells. The origins of the energy should coincide among the supercells, that is, the local potential in the most remote atom from a defect has the same value among the supercells. The local potential is the screened one and includes bare ion, Hartree, and exchange correlation potentials. To evaluate the local potential at the supercell boundary, we calculate the average local potential within a sphere of radius 1.6 Bohr centered on an Si atom near the vertex of the cubic supercell. Figure 1 shows the results for cubic supercells of 64, 216, 512, 1000, and 1728 Si atoms. The potential origin is set to that of pure Si crystal for each supercell size. The horizontal axis refers to the number of atoms per supercell for pure Si crystal. The circles, triangles, squares, and diamonds indicate the B_s, ICO B_{12}, OCT B_6, and ⟨001⟩B-Si defects, respectively. These defects are described in Sec. III. Closed and open symbols refer to the neutral and charged states, respectively. The charged defects are B_s^-, ICO B_{12}^{2-}, OCT B_6^{2-}, and ⟨001⟩B-Si^+. As shown in Fig. 1, the convergence for OCT $B_6^{0,2-}$ and ⟨001⟩B-Si^+ is slower than that for the other defects. We also show the supercell size dependence of the XPS binding energy in Fig. 2. From these figures, while the supercell with 512 Si atoms achieves convergence within 0.1 eV, which is our criterion of accuracy, we adopt a supercell of 1000 Si atoms in this work. As for the formation energy, the energy differences between the supercells of 1000 and 1728 Si atoms are less than 0.03 eV except for the ICO $B_{12}^{0,2-}$. The differences for ICO $B_{12}^{0,2-}$ are 0.14 eV.

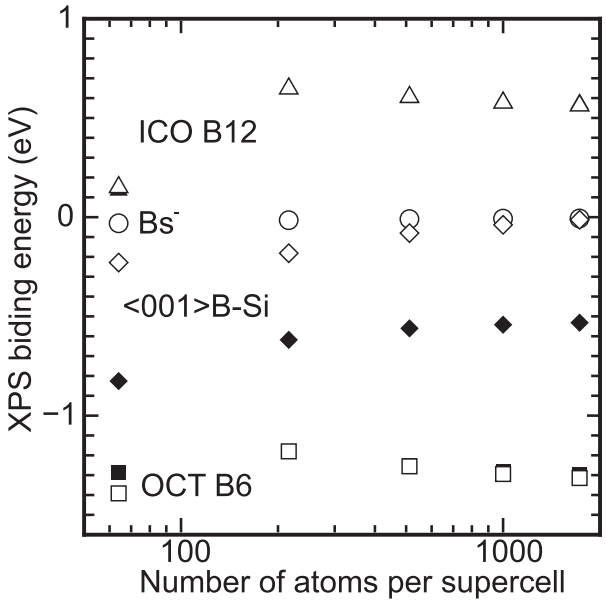

FIG. 2. Supercell size dependence of XPS binding energy. The horizontal axis refers to the number of atoms per supercell for pure Si crystal. The origin of the XPS binding energy is that of the substitutional B (B_s) in the neutral state. The symbols are the same as in Fig. 1. Closed and open symbols refer to the neutral and charged states, respectively.

For the charge state calculation, we consider the energy correction. The Makov–Payne correction is well known in this field.[22] While the correction gives very accurate results for atoms and molecules, the correction is overestimated for the calculation of defects.[23,24] Next we considered the correction proposed by Laks and coworkers.[23,25] This correction adjusts the formation energy of charged states by adding ΔV into the electron chemical potential. ΔV is the difference between the local potential of the most distant atom from the defect and that of an atom in the pure substrate crystal. In Fig. 1, the average local potential difference for the neutral and charged states corresponds to this correction (ΔV) for each supercell size. The qualitative direction of ΔV correction is reasonable, which increases the formation energy. However, it is not found that the correction clearly enhances the convergence of the formation energy with respect to the supercell size. In this study, the results for the charged states do not include any correction due to the aforementioned reason and the smallness of ΔV.

III. MODELS

In this section, we describe the models used for the XPS calculation of B 1*s*. The models are based on theoretical and/or experimental proposals, and are classified into three groups: defects including one or two boron atoms, polyhedral boron clusters, and vacancy-related defects. The optimized atomic configurations for defects in the neutral and spinless states are shown in Fig. 3.

A. Defects including one or two boron atoms

Substitutional B (B_s) is the most important and common defect in silicon (Si), which generates holes and is used as the *p*-type dopant for Si-based devices.

Interstitial B at hexagonal site (B_i@H) is in a metastable configuration. The hexagonal (H)-site is the center position of the Si six-membered ring. On the other hand, the tetrahedral (T)-site, which is tetrahedrally surrounded by four Si atoms, is unstable for the interstitial B atom.

⟨001⟩B-Si is the configuration where a B-Si pair aligned along the ⟨001⟩ direction occupies one Si site in the crystal. In this configuration, the B has a coordination number of 3.

B_s-Si@T refers to the configuration of a substitutional B atom with an interstitial Si atom around the T-site.

Bond center B (bcB) is the configuration where a B atom is located at the bond center connecting the two nearest-neighbor substitutional Si atoms.

B_s-B_s is a B cluster consisting of two nearest-neighbor substitutional B atoms. The existence of this cluster as well as B_s was proposed on the basis of infrared experiments.[26] Later, the interpretation of the modes was corrected on the basis of a first-principle calculation.[6]

⟨001⟩B_2 split is a B cluster where two B atoms are aligned along the ⟨001⟩ direction and occupy one substitutional site. This cluster was theoretically suggested by Tarnow,[27] and investigated as a possible immobile and electrically inactive cluster, which was suggested on the basis of B diffusion experiments, by first-principles calculation by Zhu *et al.*[28] Vailionis *et al.* proposed the existence of this cluster because the density of the sp^2 state, which is contained in the ⟨001⟩B_2 cluster, increases with the B concentration according to the results of near-edge X-ray absorption fine-structure spectroscopy (NEXAFS).[29] While the infrared spectra of this cluster have been known since 1960s, the signals were misinterpreted as those by the defects including only one B atom.[26] A first-principles frozen phonon calculation showed that the characteristic structure of the ⟨001⟩B_2 split causes isotope shifts similar to those by the defects including one B atom.[6]

B. Polyhedral boron clusters

Boron is an interesting element and takes exotic atomic configurations in nature, such as polyhedra.[10] Cubic metal hexaborides MB_6, where *M* is an alkaline earth metal, lanthanide, or actinide, are composed of octahedral B_6 clusters. Some metal dodecaborides MB_{12} have cubo-octahedral B_{12} as a unit of the structure. The icosahedral B_{12} cluster is a unit of simple substance of B and boron carbides. The reason for B taking such exotic structures is that small atoms such as B preferentially form triangular structure and undergo three-center bonding, where two electrons occupy a triangular orbital surrounded by three atoms. Thus, it is expected that some of the B atoms in silicon crystal will form polyhedral clusters. The following polyhedral cluster models are considered in this work.

Tetrahedral B_4 (TETRA B_4) is a cluster where a B_4 tetrahedron occupies one Si substitutional site and has four bonds to the nearest-neighbor Si atoms. This cluster is the smallest polyhedral cluster that consists of triangular faces with each B atom at the vertex and has four bonds to the nearest-neighbor Si atoms; this cluster is not based on experimental or theoretical proposals.

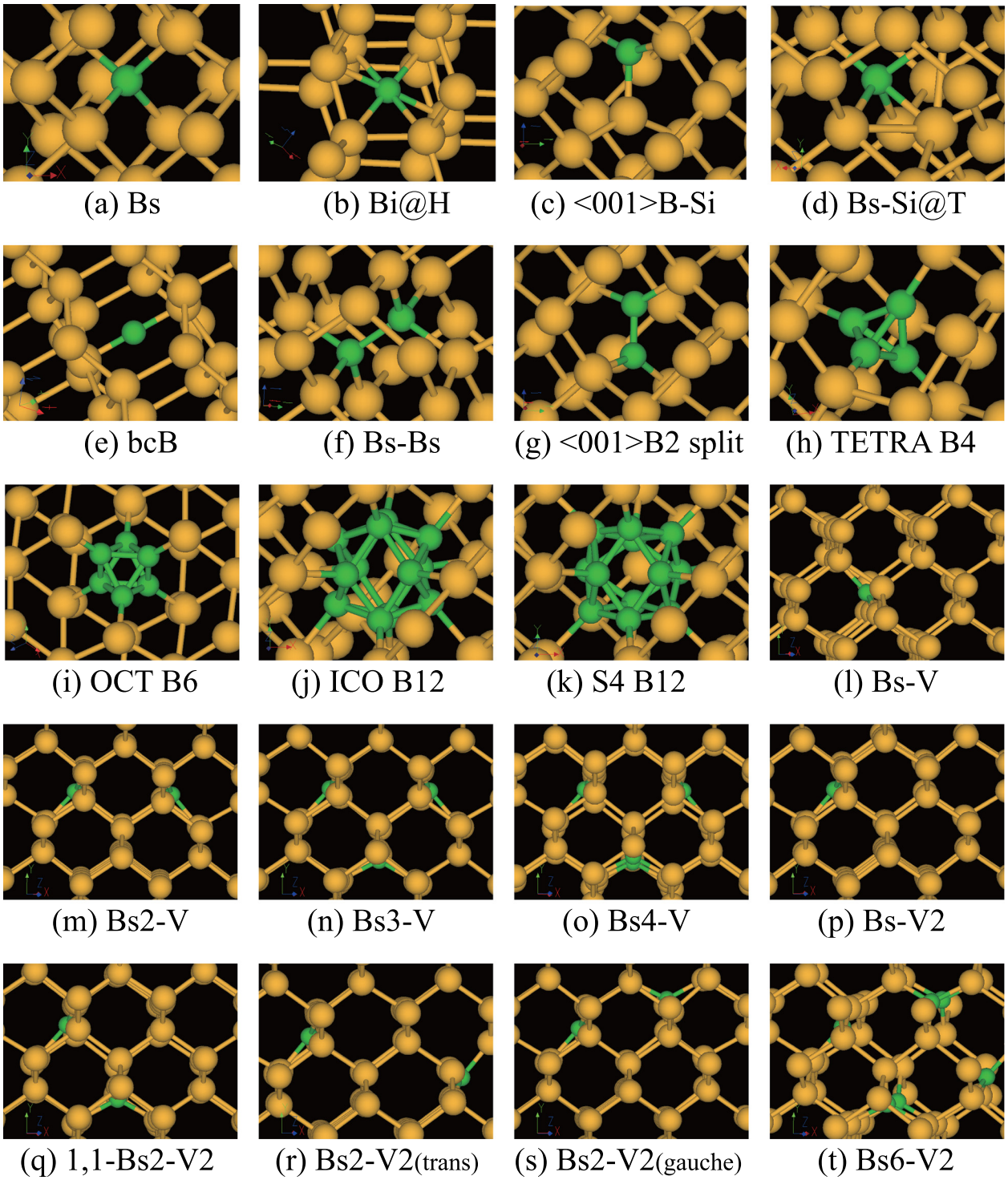

FIG. 3. Optimized atomic structures of defects in the neutral and spinless state. Yellow and green balls refer to Si and B atoms, respectively. The x, y, and z axes in each figure correspond to [100], [010], and [001] directions, respectively. About the abbreviations for the defect structures, see Section III.

Octahedral B_6 (OCT B_6) is the B_6 cluster which occupies two adjacent Si substitutional sites and has six bonds between the nearest-neighbor Si and vertex B atoms. OCT B_6 was theoretically proposed by Ohmori *et al.* to explain the XPS peak[8] observed for B-implanted Si substrates by Mizushima *et al.*[4]

There are three types of B_{12} cluster in Si: icosahedral (ICO), cubo-octahedral (CO), and S_4 clusters (Fig. 4).

Regular ICO and CO clusters are easily formed using a cube with different values of the parameters u and v. On each face of the cube, we draw one line parallel to the edges and through the center of the face in such a way that no lines are connected to each other, and place twelve B atoms on the lines so that the distance between each B atom and the face center is v as shown in Figs. 4(a) and 4(b). The length of the edges is $2u$. We obtain the regular icosahedron and cubo-octahedron when $v/u = (\sqrt{5}-1)/2$ and $v/u = 1$, respectively. In Si crystal, these clusters occupy five Si atoms, that is, an Si atom and its four nearest-neighbor atoms, and are distorted by the surrounding Si atoms. Roughly speaking, the

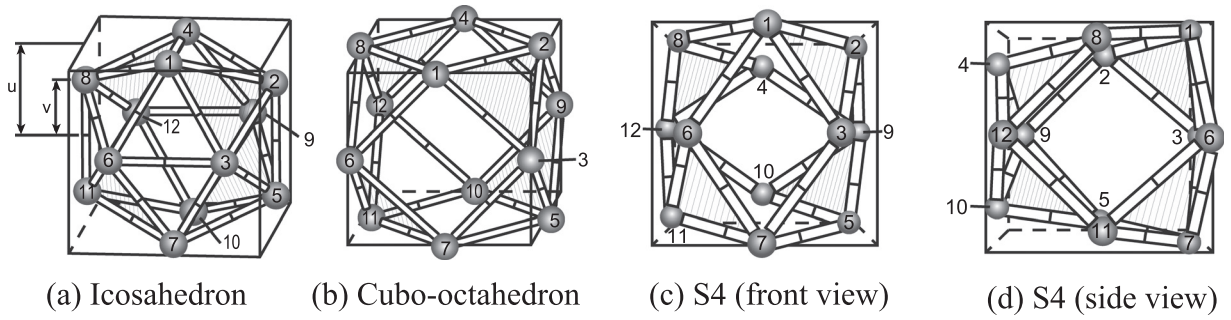

FIG. 4. Schematic structures of B_{12} clusters. The length of the edges of the cube is $2u$ and the distance between each B atom and the center of the face is v. We obtain the regular icosahedron (a) and cubo-octahedron (b) when $v/u = (\sqrt{5}-1)/2$ and $v/u = 1$, respectively. The S_4 cluster has the S_4 symmetry and its front view (c) and side view (d) are shown.

center of the CO, ICO, and S_4 B_{12} clusters is the center atom of the removed Si cluster, and the hatched regions in Fig. 4 correspond to the four outer Si atoms of the removed Si cluster. Therefore, each B atom of these B_{12} clusters is connected to one dangling bond from the remaining Si atom and all the dangling bonds of the remaining Si atoms are terminated. Mizushima *et al*. first proposed the ICO B_{12} cluster in silicon on the basis of XPS, infrared (IR) spectroscopy, and sheet carrier measurements.[4] The detailed electronic and atomic structures of the ICO cluster were determined by first-principles calculation.[6] The frozen phonon calculation has also been carried out and IR spectra have been calculated for the ICO cluster.[6] These calculation results support the experimental observations.

For the CO B_{12} cluster, two different groups obtained opposite conclusions, which were reported almost simultaneously.[6,30] Okamoto *et al*. reported that CO B_{12} is the most stable among the B_{12} clusters.[30] In contrast, Yamauchi *et al*. revealed that CO B_{12} is not a locally minimal configuration in energy, but exists at a saddle point between the ICO and S_4 B_{12} configurations on the basis of a frozen phonon calculation.[6,7] We carried out the frozen phonon calculation using more reliable condition of a $3 \times 3 \times 3$ sampled k-mesh than that of the single Γ point in Ref. 7 and reconfirmed that the CO cluster is at the saddle point. This discrepancy between the results of the two groups was because the calculations by Okamoto *et al*. were under the artificial C_{3v} symmetry, meaning that CO B_{12} could not decay to the ICO or S_4 cluster. Therefore, the CO B_{12} cluster is not adopted as a model.

In addition, Higashiguchi *et al*. reported that the symmetry of CO B_{12} was lowered from O_h to T_d by the energy optimization using an $Si_{165}H_{100}$ base cluster model.[31] This is because the symmetry T_d, which is included in O_h, was kept during the optimization, and prevented the CO B_{12} from decaying to ICO or S_4 cluster.

As shown in Figs. 4(c) and 4(d), the S_4 structure has lower symmetry (S_4) than the regular ICO and CO structures. The S_4 symmetry has an operation of a $\pi/2$ rotation followed by a reflection in the plane perpendicular to the rotation axis. From the symmetry, there are three types of atoms in the S_4 cluster. In the figure, the atoms numbered one, two, and three are all inequivalent.

The aforementioned polyhedral B clusters: TETRA B_4, OCT B_6, ICO, and S_4 B_{12} terminate all the dangling bonds of surrounding Si atoms and make Si-B bonds, whose number is the same as that of B atoms. For example, the S_4 B_{12} has twelve Si-B bonds with the surrounding Si atoms.

C. Defects including vacancies

Uedono *et al*. probed defects in plasma-immersed B-implanted Si using a monoenergetic positron beam combined with first-principles analysis as well as XPS measurement. They found that for as-doped samples, the vacancy-rich region was localized at a depth of 0–10 nm from the surface and that the major defect species were divacancy-B complexes.[12]

We considered two different defect models with one vacancy and two adjacent vacancies. There are four types of defects with one vacancy: one vacancy with n nearest-neighbor substitutional B atoms: ($B_s n$-V, $n = 1$–4). For the defects with two vacancies, we considered the two adjacent vacancies with the n nearest-neighbor substitutional B atoms ($B_s n$-V2), where $n = 1$, 2, and 6. The reason that we did not deal with n of 3–5 is that such defects have a fairly high formation energy and that the aforementioned models are sufficient to determine the trend of XPS binding energies. In the case of $n = 1$, n is omitted. B_s2-V2 has three different configurations depending on the two B positions. One (1,1-B_s2-V2) is the configuration where the two B atoms are in the substitutional sites that are originally connected to the same removed Si atom. In the other two models, B_s2-V2(trans) and B_s2-V2(gauche), the two substitutional B are in sites that are connected to different removed Si atoms. B_s2-V2(trans) and B_s2-V2(gauche) are named from their use in chemistry, where trans and gauche refer to the configurations with dihedral angles of 60° and 180° for the two B and the two removed Si atoms, respectively.

IV. RESULTS

Hereafter, we adopt the B 1*s* core-level XPS binding energy of non-spin-polarized substitutional B (B_s) as the origin for the binding energy and discuss the relative shift, where a positive (negative) value refers to a larger (smaller) binding energy than that of B_s. For the formation energy, we also adopt that of non-spin-polarized B_s as the origin and discuss the relative values.

TABLE II. Relative formation and B 1*s* core-level XPS binding energies for boron defects. The origin of the energies is that of the non-spin-polarized substitutional boron (B_s). Δspin refers to the difference between the numbers of electrons with up and down spins. The Fermi energy is set to the valence band top. ΔV is the difference between the local potential average of the most distant atom from the defect and that of an atom in the pure Si crystal.

	Neutral state			Charged state			
	Δspin	Formation energy (eV)	XPS BE (eV)		Formation energy (eV)	XPS BE (eV)	ΔV (eV)
B_s	0	0.00	0.00	B_s^-	0.00	−0.01	−0.02
	1	0.00	0.00				
B_i@H	0	3.09	0.66	$B_i@H^+$	2.97	0.82	0.01
	1	3.00	0.91				
⟨001⟩B-Si	0	2.94	−0.54	⟨001⟩B-Si^+	2.45	−0.04	0.02
	1	2.89	−0.61				
B_s-Si@T	0	2.60	1.21	B_s-Si@T^+	1.96	1.31	0.01
	1	2.60	1.20				
bc(bond-center)B	0	3.36	0.49	bcB^+	2.77	1.08	0.02
	1	3.35	0.13				
B_s-B_s	0	0.78	−0.06	$B_s - B_s^{2-}$	0.81	−0.11	−0.05
⟨001⟩B_2 split	0	0.79	0.08				
TETRA B_4	0	3.05	−0.29				
OCT B_6	0	−0.80	−1.28	$(OCT\ B_6)^{2-}$	−0.80	−1.29	−0.03
ICO B_{12}	0	−4.51	0.58	$(ICO\ B_{12})^{2-}$	−4.53	0.58	−0.05
(S_4 B_{12})-1	0	−3.85	−0.11	$(S_4\ B_{12})^{2-}$−1	−3.85	−0.11	−0.05
(S_4 B_{12})-2			0.40	$(S_4\ B_{12})^{2-}$−2		0.39	
(S_4 B_{12})-3			0.60	$(S_4\ B_{12})^{2-}$−3		0.60	
B_s-V	0	3.47	0.26	B_s-V^+	3.15	0.47	0.01
	1	3.32	0.28				
B_s2-V	0	2.80	0.42				
B_s3-V	0	2.83	0.29	B_s3-V^-	2.79	0.30	−0.02
	1	2.83	0.30				
B_s4-V	0	2.54	0.25	B_s4-V^{2-}	2.86	−0.22	−0.04
B_s-V2	0	5.16	0.32	B_s-$V2^-$	5.34	0.35	−0.03
	1	5.10	0.27				
1,1-B_s2-V2	0	4.98	0.38				
B_s2-V2(trans)	0	4.44	0.43				
B_s2-V2(gauche)	0	4.59	0.47				
B_s6-V2	0	3.91	0.46	B_s6V2^{2-}	4.45	−0.11	−0.04

The formation energy E_{form} of n_B B, n_{Si} Si atoms, and n_e electrons, is defined as follows:

$$E_{\text{form}} = E[n_B, n_{Si}, n_e] - n_B\mu_B - n_{Si}\mu_{Si} - n_e\mu_e,$$

where E is the total energy calculated in the 1000-atom supercell and μ_B, μ_{Si}, and μ_e are the chemical potentials for B, Si, and electrons, respectively. μ_{Si} and μ_B are set to the energy per atom of Si crystal and B_s, that is, $\mu_{Si} = E[\text{Si}]/1000$ and $\mu_B = E[B_s] - 999\mu_{Si}$, where $E[\text{Si}]$ and $E[B_s]$ are the total energies calculated in the 1000-atom supercell for pure Si crystal and B_s, respectively. Since the ion-implanted and plasma-doped Si wafers are considered, where the region deep from the surface is bulk Si with few B atoms, it is reasonable to take the energy of B_s as μ_B, which corresponds to the B-dilute and Si-rich limit. In this study, μ_e is the Fermi energy and is set to the energy of the valence band top of the Si crystal.

We consider spin polarization for the neutral configurations with odd numbers of electrons in the gap states, and the difference between the numbers of up- and down-spin electrons is denoted by Δspin. In the spinless calculation, there are no defects with doubly degenerated highest occupied orbitals with two electrons or triply degenerated highest occupied orbitals in the band gap. Thus, we only consider the case of Δspin = 1. Charged states are examined for the configurations with the possibility of being charged when the Fermi energy is set to that of the valence band top. Such configurations have occupied states above the valence band top and/or empty states near the valence band top.

In Table II, we summarize the calculated formation energies and XPS binding energies for the B defects in Si.

Overall, the spin polarization slightly decreases the formation energy. The largest change is 0.15 eV for B_s-V. In terms of the XPS binding energy, the spin polarization effect is not in one direction. The positive and negative largest differences in the binding energy between the polarized and non-polarized configurations are +0.25 for B_i@H and −0.36 eV for bcB, respectively.

In terms of the charge effect, compared with the neutral states, the positively charged states such as B_s-Si@T^+ have a considerably lower formation energy, and most of the negatively charged states have a slightly higher energy. The

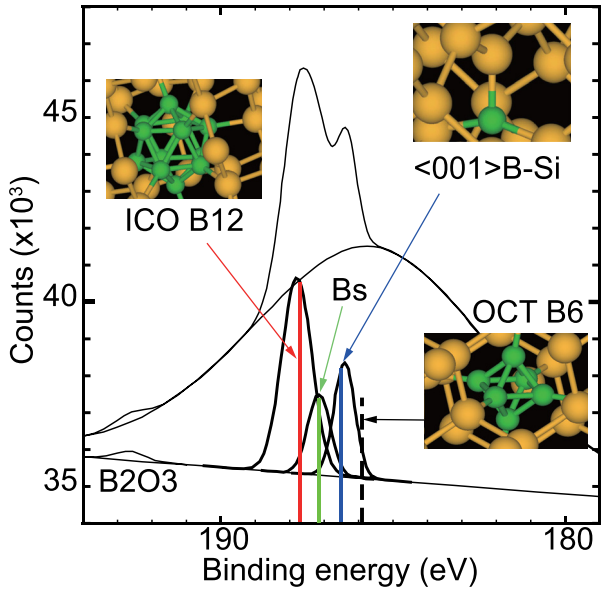

FIG. 5. B 1*s* core-level XPS spectra of B clusters. Experimental and deconvoluted data are from Mizushima *et al.*[4] (black lines). Vertical lines indicate the values calculated by the ΔSCF method for icosahedral B_{12} (red), substitutional B (green), ⟨001⟩B-Si (blue), and octahedral B_6 (black dashed). The substitutional B lines are adjusted so that the experimental and calculated values match.

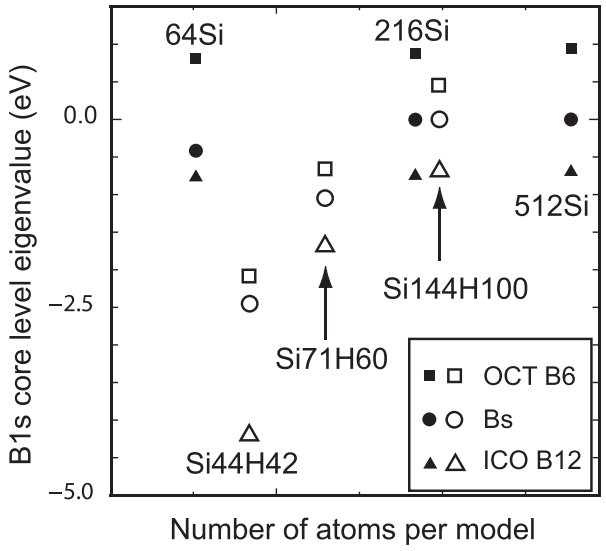

FIG. 6. Model size dependence of the B 1*s* core-level XPS binding energy of B clusters calculated by the STS method. Open and closed symbols refer to the cluster and supercell model calculations, respectively. The origin of the eigenvalues is set to that of substitutional B using the largest model for both models.

neutral defects corresponding to the positively charged states have occupied electronic levels in the band gap and their formation energy is decreased by the release of electrons. Those for the negatively charged states have empty or partially filled electronic levels near the valence band top, which do not contribute to the decrease in the formation energy, and their formation energy is increased by the electron–electron repulsion resulting from the acceptance of electrons.

In a *p*-type substrate, where the Fermi energy is near the valence band top, the electrical activity of defects is easily evaluated by comparing the formation energy between the neutral and charged states in Table II. Charged states with the formation energy lower than or roughly equal to that of the neutral state are preferentially charged states. Among these charged states, negatively charged states generate holes and are electrically active, and positively charged states annihilate holes and decrease electrical activity. The other defects, whose charged states have higher energy than the neutral states, are electrically inactive.

Regarding the XPS binding energy, the effects of the charged state reveal a simple trend that the positively charged states increase the binding energy and the negatively charged states decrease the energy compared with the neutral state. This trend can be simply understood by the change in electrostatic potential.

The spin polarization and charged states hardly affect the defects whose relevant states have shallow levels and widely spread wave functions, such as B_s, B_s-B_s, OCT B_6, ICO B_{12}, and S_4 B_{12}.

As expected, the polyhedral B clusters have negative formation energies except the artificial model of TETRA B_4. In particular, ICO B_{12} has the most negative value of −4.51 eV. The ICO B_{12} cluster has only one inequivalent B site due to the symmetry. The S_4 B_{12} cluster has three inequivalent B sites, which are referred to as 1, 2, and 3. These numbers indicate the atom number of S_4 B_{12} in Figs. 4(c) and 4(d).

The XPS binding energies for the defects including vacancies are distributed in a narrow region from 0.25 to 0.47 eV. This is probably because they have the same local structure where the substitutional B atoms are adjacent to vacancies.

V. DISCUSSION

From the formation energy analysis, the B_s-B_s and ⟨001⟩B_2 split defects have much lower energy than the other defects with interstitials and have actually been detected in IR absorption experiments. In XPS experiments, however, they are difficult to detect, because their binding energies (−0.06 and 0.08 eV) are near that of B_s.

In Fig. 5, we show the experimental XPS spectra and deconvoluted peaks for the B-ion implanted silicon substrate by Mizushima *et al.*[4] They suggested that the middle peak, which is the origin of the relative XPS binding energy, is due to the substitutional B (B_s) and that the higher (H) peak of +0.6 eV and the lower (L) peak of −0.7 eV originate from ICO B_{12} and a threefold coordinated defect, respectively. It was also reported that the defects of the H peak are electrically active and that of the L peak is not active. The XPS peaks calculated by the ΔSCF method are drawn as vertical lines for ICO B_{12}, B_s, ⟨001⟩B-Si, and OCT B_6, whose binding energies are 0.58, 0.00, −0.61, and −1.28 eV, respectively. The structures of these clusters are shown in the inset. The XPS peaks at 0.6 and −0.7 eV are in excellent agreement with the peaks of ICO B_{12} and ⟨001⟩B-Si, respectively. ⟨001⟩B-Si is a threefold coordinated defect and is electrically inactive, which is consistent with the results of the experiment by Mizushima *et al.*[4] From the viewpoint of the formation energy (Table II), if ⟨001⟩B-Si is detected, then ⟨001⟩B-Si^+ should also be detected, which has lower formation energy than the neutral state. Unfortunately, the XPS

binding energy for ⟨001⟩B-Si$^+$ is near the energy origin of B_s and it is difficult to distinguish ⟨001⟩B-Si$^+$ and B_s. Although the calculated XPS binding energies for ICO B_{12}, B_s, and ⟨001⟩B-Si agree well with those by experiments, the populations deconvoluted from experiments do not necessarily agree with the population that would be predicted by the formation energies in Table II. For example, considering the formation energies 0.00 and 2.94 eV for B_s and ⟨001⟩B-Si, respectively, the population of B_s should be larger than that of ⟨001⟩B-Si. This discrepancy is probably because the populations are determined by the initial dynamical process to form defects, and because the sample is the as-implanted Si wafer without annealing and far from thermal equilibrium.

On the other hand, on the basis of the same experimental data, Ohmori *et al*. suggested different assignments, where the H peak corresponds to OCT B_6 cluster. They obtained binding energy of 0.3 eV for the OCT B_6[8] and binding energies of 0.4 and 0.9 eV for OCT B_6 and ICO B_{12},[9] respectively, by the STS method using the DV-Xα method and cluster models, where the Si substrate is modeled by Si clusters whose dangling bonds at the surface are terminated by hydrogen atoms. The discrepancy between their and our results is due to the use of different cluster models for OCT B_6 and other clusters as well as the small cluster size. We confirmed their results by performing a cluster model calculation by the STS method with the PWCs. In Fig. 6, the B 1*s* eigenvalues in the STS calculation are shown for OCT B_6, B_s, and ICO B_{12} using the cluster and supercell models. For the same system size, the convergence of the eigenvalues, that is, the XPS binding energy, in the supercell models is much more rapid than that in the cluster models. However, in the cluster models, the order of the XPS binding energy for the defects is the same for each model cluster size. In Refs. 8 and 9, Ohmori *et al*. compared the eigenvalues of OCT B_6 and B_s calculated using the $Si_{44}H_{42}$ and $Si_{71}H_{60}$ cluster models, respectively. Therefore they obtained the contradictory results.

In addition to the above-discussed clusters in ion implanted samples, we also identified B defects in the plasma-doped samples. For B defects in an Si substrate prepared by plasma doping, Tsutsui *et al*. studied the chemical bonding state by soft XPS and the depth profile of the carrier concentration by combining Hall measurement and step-by-step etching. They found three soft XPS peaks, which are referred to as the highest binding energy (BEH), the middle binding energy (BEM), and the lowest binding energy (BEL), where BEL is electrically active and has a wide depth profile, while BEM and BEH are electrically inactive and exist only near the surface.[11] Assuming that BEL is due to B_s, the relative XPS binding energies of BEH, BEM, and BEL are 2.5, 1.2, and 0.0, respectively. We assigned BEM to B_s-Si@T, that is, the complex of substitutional B and interstitial Si near the T-site, because its theoretical XPS binding energies are 1.21 and 1.31 eV for the neutral and charged states, respectively, and its calculated electrical activity is consistent with that observed experimentally. For BEH, no candidate has been found among the analyzed models.

Uedono *et al*. probed vacancy-type defects in plasma-immersed B-implanted Si using a monoenergetic positron beam combined with first-principles analysis as well as XPS measurement. They found that, for as-doped samples, the vacancy-rich region was localized at a depth of 0–10 nm from the surface and that the major defect species were divacancy-B complexes.[12] Figure 7 shows the experimental data for the as-doped sample and the calculated XPS binding energies. We calculated the XPS peaks for complexes of mono/divacancy and substitutional B atoms (B_sn-V2, $n = 1$, 2, 6/B_sm-V, $m = 1$–4). The XPS binding energies from these defects are located in the arrow-marked region in green. Considering the charged states as well as the neutral states results in the arrow-marked region being wider than that in the previous work.[13] In particular, the XPS binding energy of the most energetically stable B_s2-V_2-type defect is indicated by a vertical thick blue line. The calculated results are consistent with the existence of divacancy-B complexes, although there appear to be various other types of defect. However, it should be noted that the experimental XPS spectra are not necessarily due to vacancy-related defects because the positron measurement is very sensitive to vacancies. Assuming that the electrically active peak at 187.1 eV for the annealed sample in Ref. 12 is due to substitutional B, the relative XPS binding energies for the deconvoluted peaks at 187.9 and 186.7 eV in the as-implanted samples are +0.8 and −0.4 eV, respectively. Considering that the number of interstitial defects in as-doped samples is larger than that in annealed samples, the peaks at 187.9 and 186.7 eV may be due to B_i@H (0.66, 0.91, and 0.82 eV for non-spin-polarized, spin-polarized, and charged states) and ⟨001⟩B-Si (−0.54 and −0.61 for non-spin-polarized and spin-polarized states), respectively. It has been reported that after annealing, the 187.9 and 186.7 eV peaks disappear and BEL and BEM peaks emerge.[12] It is reasonable that shortly after the deposition process, there are many ⟨001⟩B-Si and B_i@H defects with relatively high formation energy, then after annealing, the number of more stable B_s-Si@T and B_s defects increases, while the number of high-energy defects decreases.

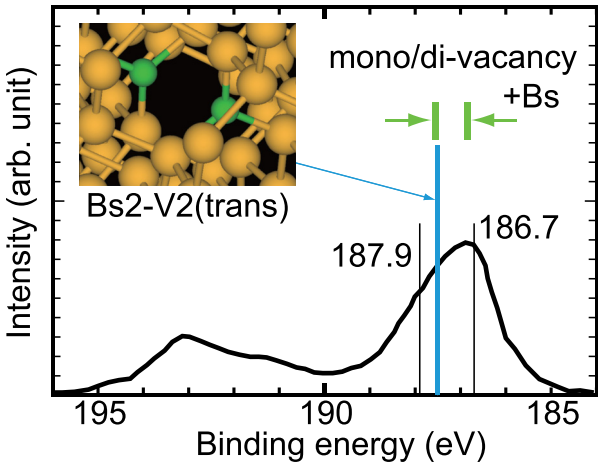

FIG. 7. B 1*s* core-level XPS binding energy of B clusters for as-doped sample obtained by plasma doping. The experimental data (black curve) and deconvoluted peaks (vertical thin black line) are from Uedono *et al*.[12] The vertical blue line indicates the calculated value for the complex with a divacancy and two substitutional B. The green arrow-marked region indicates the calculated range of various combinations of mono/divacancy and substitutional B atoms.

VI. SUMMARY

We performed a first-principles calculation of the B 1*s* core-level XPS binding energy and formation energy for B clusters in Si with high accuracy by careful evaluation of the local potential boundary condition for the defect model system. We reconfirmed that the cubo-octahedral B_{12} cluster in Si crystal is unstable and exists at the saddle point decaying to the icosahedral and S_4 B_{12} clusters. The electrically active clusters without any postannealing of ion-implanted Si were identified as icosahedral B_{12} clusters. The experimentally proposed threefold coordinated B was also identified as ⟨001⟩B-Si defects. For an as-doped sample prepared by plasma doping, complexes consisting of vacancies and substitutional B atoms consistently explain the experimental spectra. It is proposed that assuming that the XPS peak at 187.1 eV (BEL) is due to substitutional B (B_s), the experimental XPS peaks at 187.9 and 186.7 eV in as-doped samples correspond to interstitial B at the H-site (B_i@H) and ⟨001⟩B-Si defects, respectively. In the annealed samples, the complex of B_s and interstitial Si near the T-site (B_s-Si@T) is also suggested as a candidate for the experimental XPS peak at 188.3 eV (BEM).

ACKNOWLEDGMENTS

We would like to thank Dr. N. Aoki, Dr. I. Mizushima, and Dr. M. Yoshiki for helpful discussion of the experimental data and theoretical analysis. This work was supported by a Grant-in-Aid for Scientific Research (No. 22104006) from MEXT. Part of the computations was performed at the Research Center for Computational Science, Okazaki, and the Supercomputer Center, the Institute for Solid State Physics, the University of Tokyo, Japan.

[1]W. K. Hofker, Philips Res. Rep., Suppl. **8**, 1 (1975).
[2]H. Ryssel, K. Müller, K. Haberger, R. Henkelmann, and F. Jahnel, Appl. Phys. **22**, 35 (1980).
[3]S. Solmi, E. Landi, and F. Baruffaldi, J. Appl. Phys. **68**, 3250 (1990).
[4]I. Mizushima, M. Watanabe, A. Murakoshi, M. Hotta, and M. Kashiwagi, Appl. Phys. Lett. **63**, 373 (1993).
[5]I. Mizushima, A. Murakoshi, M. Watanabe, M. Yoshiki, M. Hotta, M. Kashiwagi, and M. Yoshiki, Jpn. J. Appl. Phys., Part 1 **33**, 404 (1994).
[6]J. Yamauchi, N. Aoki, and I. Mizushima, Phys. Rev. B **55**, R10245 (1997).
[7]J. Yamauchi, N. Aoki, and I. Mizushima, Phys. Status Solidi B **210**, 273 (1998).
[8]K. Ohmori, N. Esashi, M. Takao, D. Sato, and Y. Hayafuji, Appl. Phys. Lett. **87**, 112101 (2005).
[9]K. Ohmori, N. Esashi, E. Atoro, D. Sato, H. Kawanishi, Y. Higashiguchi, and Y. Hayafuji, Jpn. J. Appl. Phys., Part 1 **46**, 14 (2007).
[10]N. N. Greenwood, *Comprehensive Inorganic Chemistry* (Pergamon Press Ltd., Oxford, 1973), Vol. 1, Chap. 11.
[11]K. Tsutsui, T. Matsuda, M. Watanabe, C.-G. Jin, Y. Sakaki, B. Mizuno, E. Ikenaga, K. Kakushima, P. Ahmet, T. Maruizumi, H. Nohira, T. Hattori, and H. Iwai, J. Appl. Phys. **104**, 093709 (2008).
[12]A. Uedono, K. Tsutsui, S. Ishibashi, H. Watanabe, S. Kubota, Y. Nakagawa, B. Mizuno, T. Hattori, and H. Iwai, Jpn. J. Appl. Phys., Part 1 **49**, 051301 (2010).
[13]J. Yamauchi, Y. Yoshimoto, and Y. Suwa, Appl. Phys. Lett. **99**, 191901 (2011).
[14]J. P. Perdew, K. Burke, and M. Ernzerhof, Phys. Rev. Lett. **77**, 3865 (1996); J. P. Perdew, K. Burke, and Y. Wang, Phys. Rev. B **54**, 16533 (1996).
[15]N. Troullier and J. L. Martins, Solid State Commun. **74**, 613 (1990).
[16]D. Vanderbilt, Phys. Rev. B **41**, 7892 (1990).
[17]See http://ma.cms-initiative.jp/en/application-list/xtapp?set_language=en for the information about the code xTAPP.
[18]J. Yamauchi, M. Tsukada, S. Watanabe, and O. Sugino, Phys. Rev. B **54**, 5586 (1996).
[19]E. Pehlke and M. Scheffler, Phys. Rev. Lett. **71**, 2338 (1993).
[20]S. Kimura, J. Yamauchi, M. Tsukada, and S. Watanabe, Phys. Rev. B **51**, 11049 (1995).
[21]A. A. Bakke, H.-W. Chen, and W. L. Jolly, J. Electron Spectrosc. Relat. Phenom. **20**, 333 (1980).
[22]G. Makov and M. C. Payne, Phys. Rev. B **51**, 4014 (1995).
[23]C. G. Van de Walle and J. Neugebauer, Appl. Phys. Rev. **95**, 3851 (2004).
[24]J. Yamauchi and N. Aoki, Phys. Rev. B **71**, 205205 (2005).
[25]D. B. Laks, C. G. Van de Walle, G. F. Neumark, P. E. Blöchl, and S. T. Pantelides, Phys. Rev. B **45**, 10965 (1992).
[26]R. C. Newman and R. S. Smith, Phys. Lett. **24A**, 671 (1967); R. C. Newman and R. S. Smith in *Localized Excitations in Solids*, edited by R. F. Wallis (New York, Plenum Press, 1968), p. 177.
[27]E. Tarnow, J. Phys.: Condens. Matter **4**, 5405 (1992).
[28]J. Zhu, T. D. dela Rubia, L. H. Yang, and C. Mailhiot, Phys. Rev. B **54**, 4741 (1996).
[29]A. Vailionis, G. Glass, P. Desjardins, D. G. Cahill, and J. E. Greene, Phys. Rev. Lett. **82**, 4464 (1999).
[30]M. Okamoto, K. Hashimoto, and K. Takayanagi, Appl. Phys. Lett. **70**, 978 (1997).
[31]Y. Higashiguchi, H. Ochiai, K. Igei, K. Ohmori, and Y. Hayafuji, Jpn. J. Appl. Phys., Part 1 **46**, 467 (2007).